Supplementary Information

High output direct-current power fabrics based on air breakdown effect

Renwei Cheng[1,2,□], Kai Dong[1,2,□], Pengfei Chen[1,2], Chuan Ning[1,2], Xiao Peng[1,2],

Yihan Zhang[1,2], Di Liu[1,2] , Zhong Lin Wang[1,2,3,*]

[1] CAS Center for Excellence in Nanoscience, Beijing Key Laboratory of Micro-Nano

Energy and Sensor, Beijing Institute of Nanoenergy and Nanosystems, Chinese

Academy of Sciences, Beijing 100083, China

[2] School of Nanoscience and Technology, University of Chinese Academy of

Sciences, Beijing 100049, China

[3] School of Material Science and Engineering, Georgia Institute of Technology,

Atlanta, Georgia 30332, United States

* Corresponding Author: zlwang@gatech.edu

□ R. Cheng and K. Dong contributed equally to this work.

This file includes:

different sliding directions.

Figure S29. Output current of the FDC-TENG under different number of units.

Figure S30. Charging voltage curves of the FDC-TENG for different electrolytic capacitors.

Figure S31. The current before and after rectification.

Note S1. The measurement methods of generated charge density and residual charge density on the FEP film.

Note S2. The working mechanism of the FDC-TENG with long C.

Note S3. The calculation method of average energy conversion efficiency.

Note S4. The electrical output of the FDC-TENG with two breakdown electrodes.

Other Supplementary Material for this work includes the following:

Movie S1. (.mp4 format). Sliding the FDC-TENG to drive a watch directly.

Movie S2. (.mp4 format). Sliding the FDC-TENG to drive a commercial calculator directly.

Movie S3. (.mp4 format). Sliding the FDC-TENG to light up 99 bulbs.

Movie S4. (.mp4 format). 1053 LEDs are lit up by the FDC-TENG.

Movie S5. (.mp4 format). Heart-shaped colored lights sewn on sweater are lit up by manually sliding the FDC-TENG on the arm.

Movie S6. (.mp4 format). A hygrpothermograph is successfully driven by the FDC-TENG.
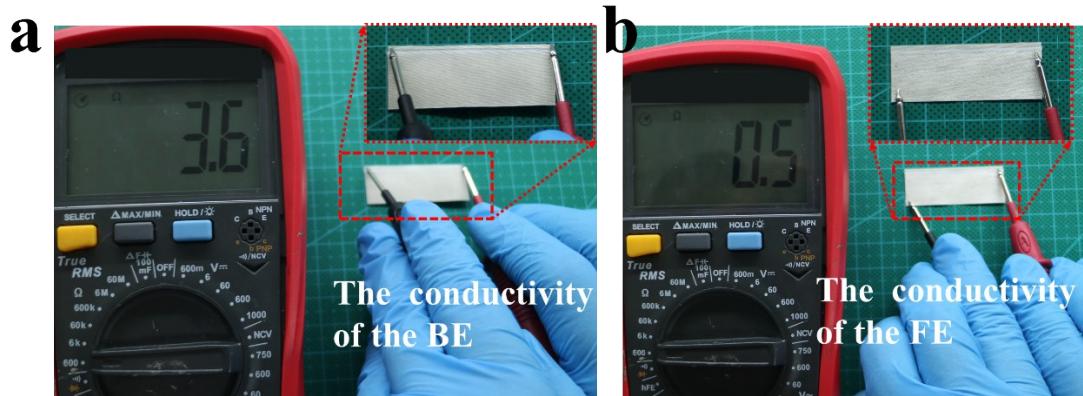
Figure S1. The excellent conductivity of the breakdown electrode (a) and friction electrode (b).

Figure S2. Test of adhesion strength between silver paste and polyester-cotton fabric.
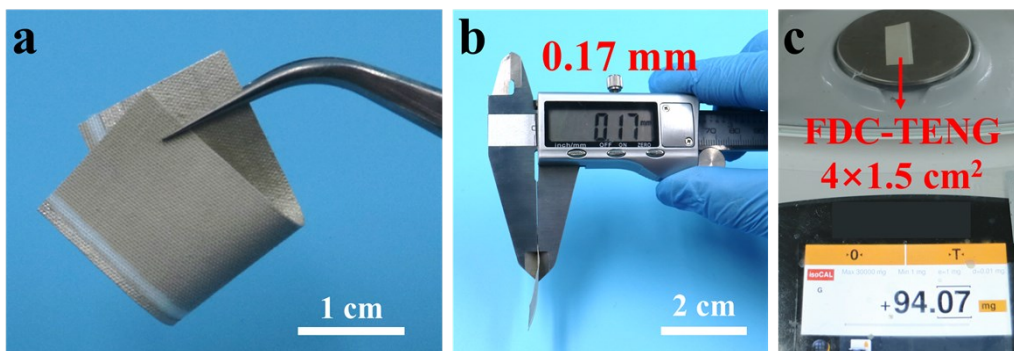
Figure S3. (a) The outstanding flexibility of the FDC-TENG. (b) FDC-TENG is thin with a thickness of 0.17 mm. (c) The lightweight characteristics of the FDC-TENG.
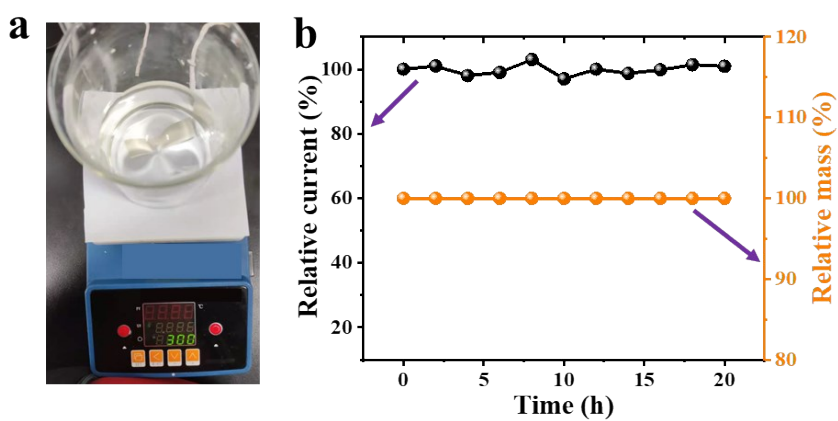
Figure S4. The washability of the FDC-TENG. (a) Photograph during washing. (b) Analysis of the washability of the FDC-TENG after 20 h washing.
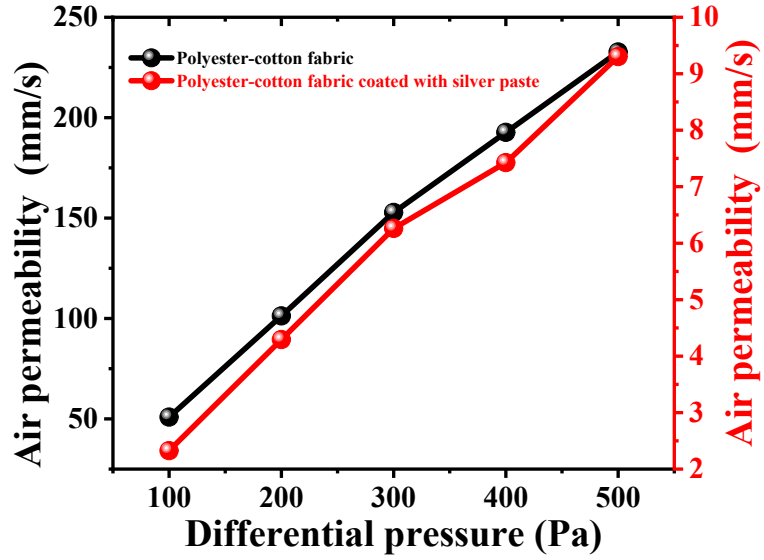
Figure S5. Differential pressure response to the air permeability of polyester-cotton fabric and polyester-cotton coated with silver paste.
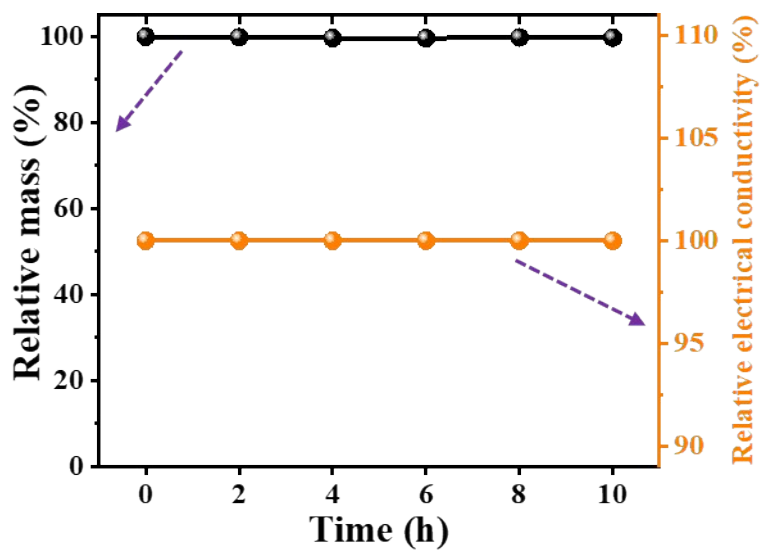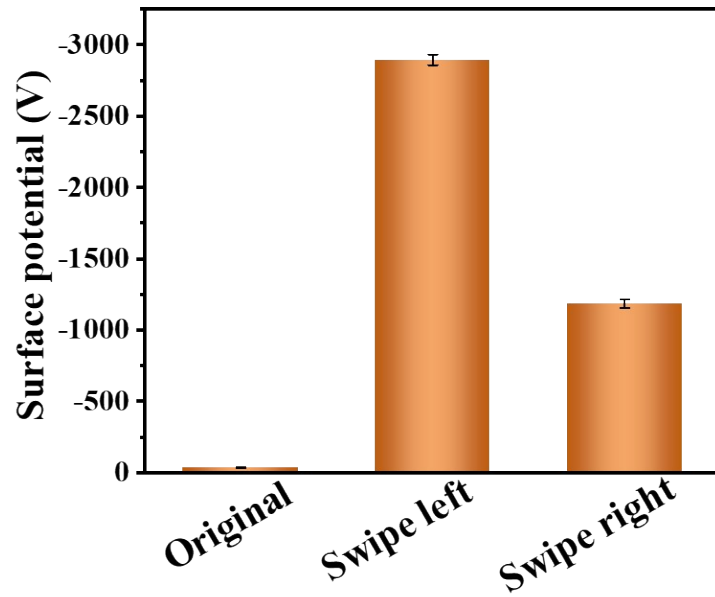

Figure S6. The surface potential of the FEP film, including three states of original, after sliding to the left, and after sliding to the right.
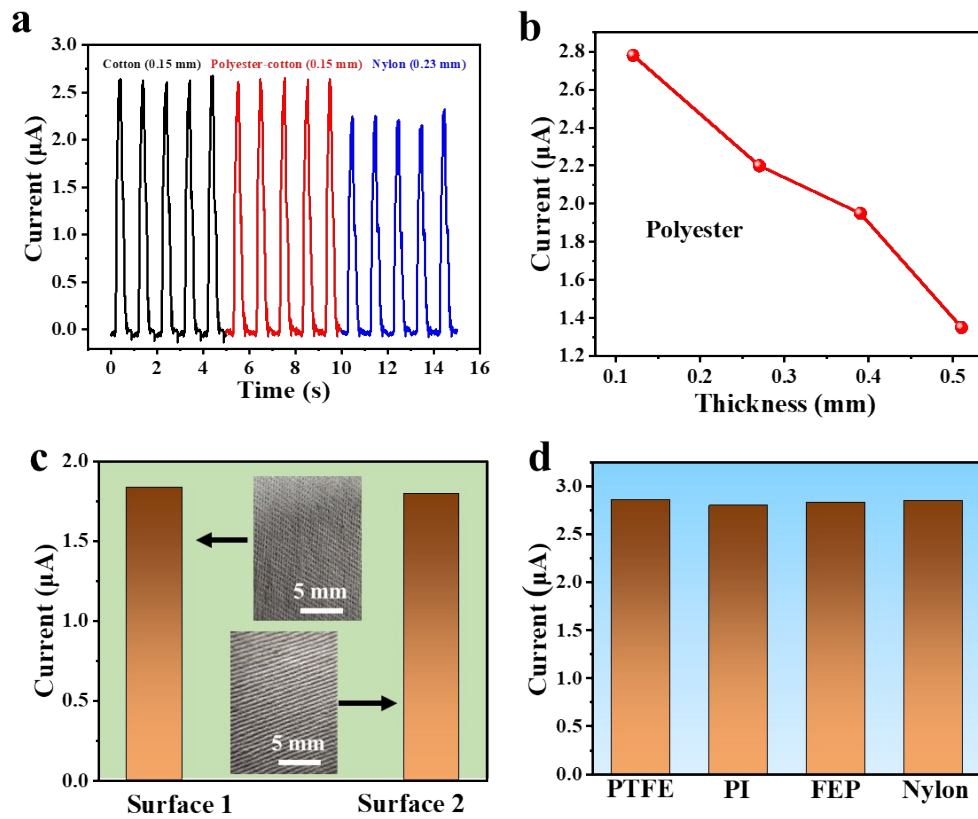
Figure S7. The influence of different substrates on the electrical output of the FDC-TENG. Output current of fabrics with different materials (a), different thicknesses (b), and different roughness (c). (d) Output current of different films.
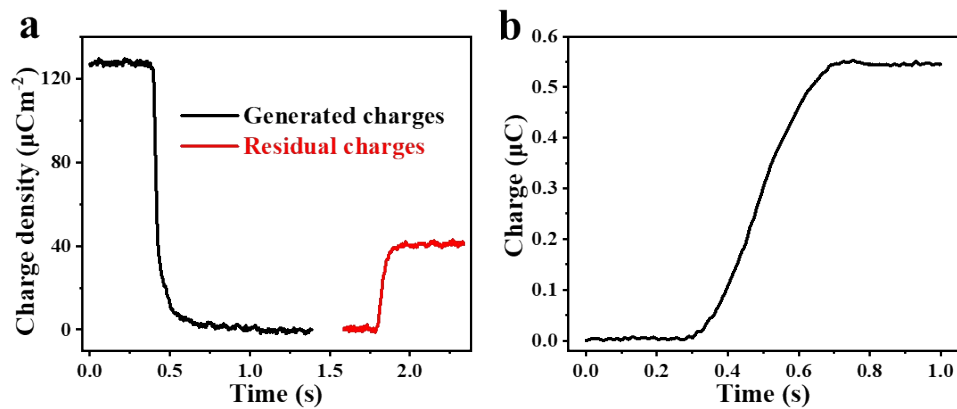
Figure S8. The generated charge density, residual charge density and harvested charges.
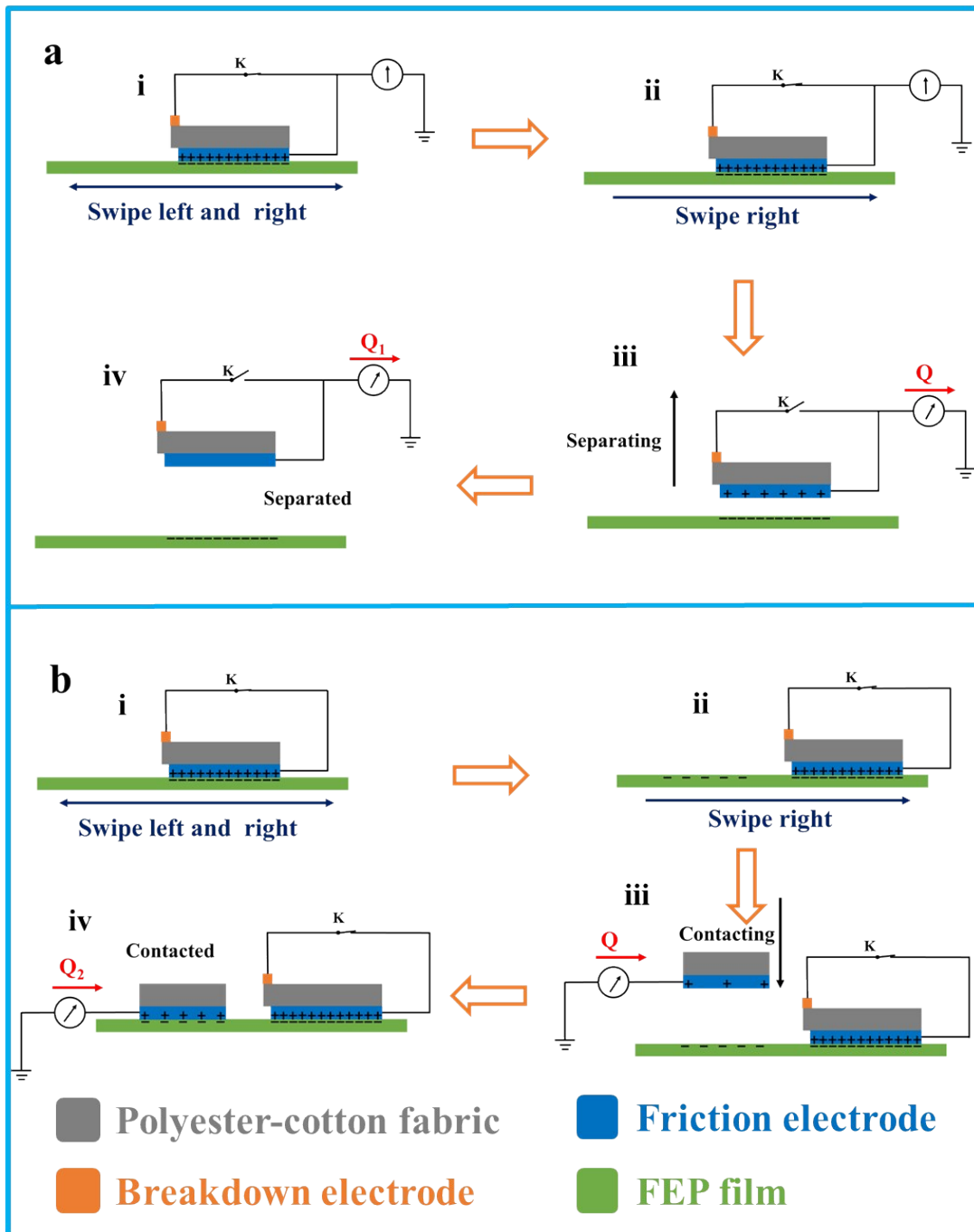
Figure S9. Schematic diagram of measurement methods of generated charges (a) and residual charges (b).
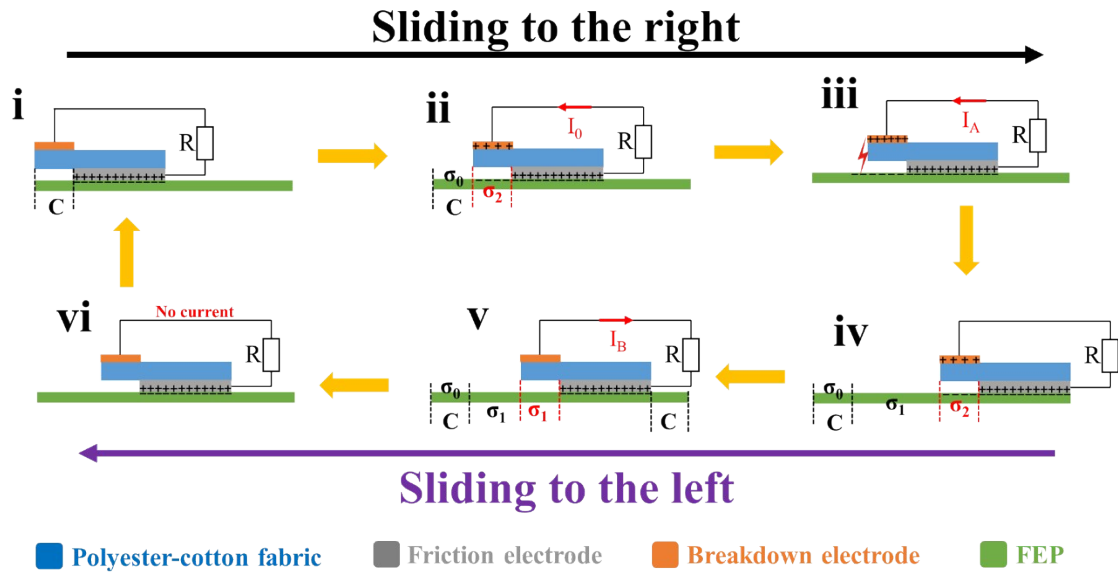
Figure S10. Schematic diagram of the working mechanism of the FDC-TENG with long width of the breakdown electrode.
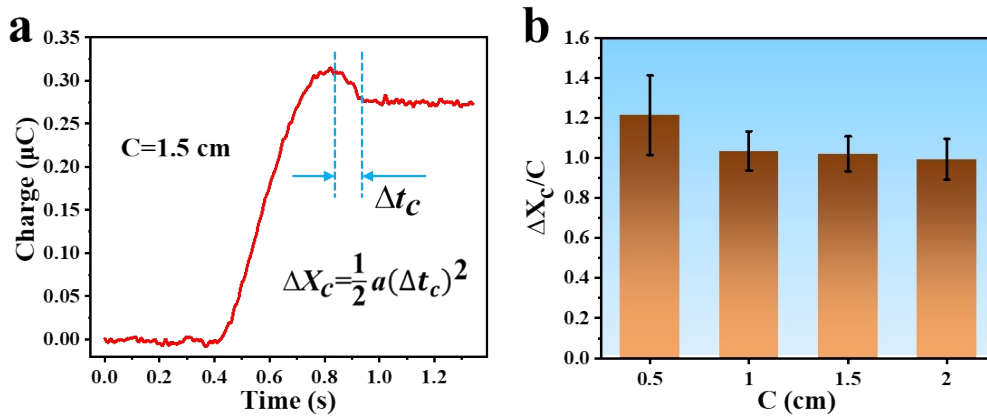
Figure S11. Causes of reverse charge. (a) The charge transfer of the FDC-TENG when C=1.5 cm. (b) The variation of $\Delta X_C/C$ with C.
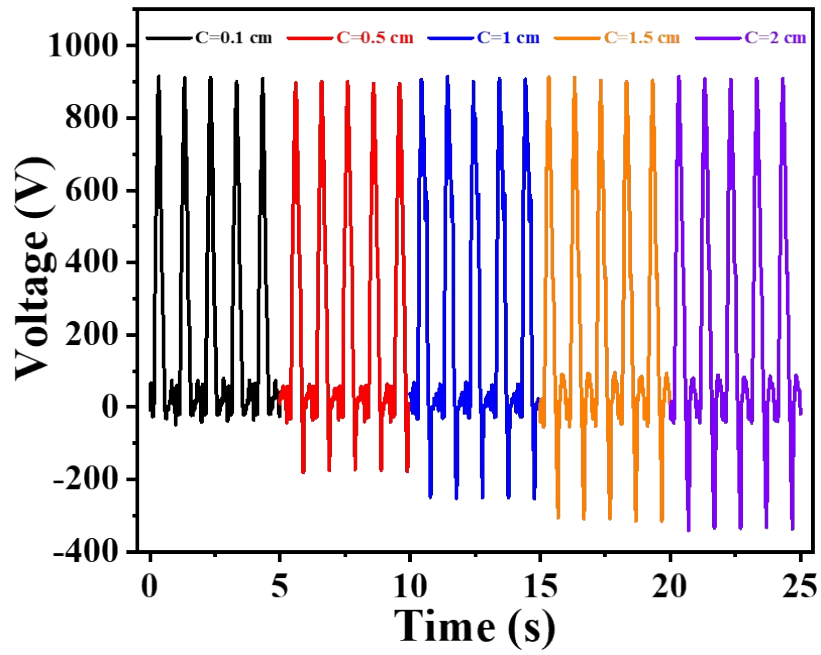
Figure S12. The voltage of the FDC-TENG with different *C* values.
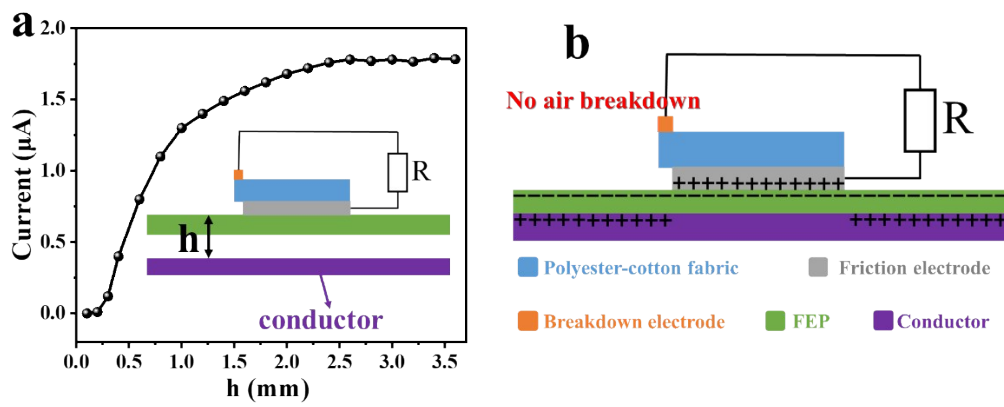
Figure S13. (a) The influence of the distance between the surface of the FEP film and the conductor on the current. (b) Schematic diagram of shielding effect.
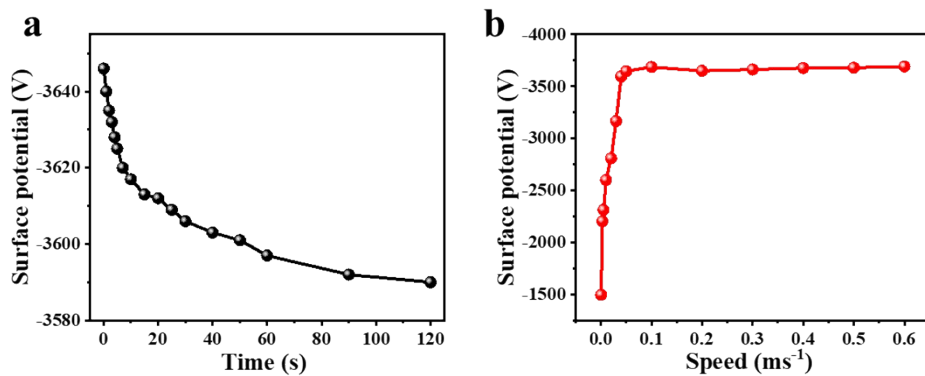
Figure S14. The relationships of surface potential of the FEP film with time (a) and speeds (b).
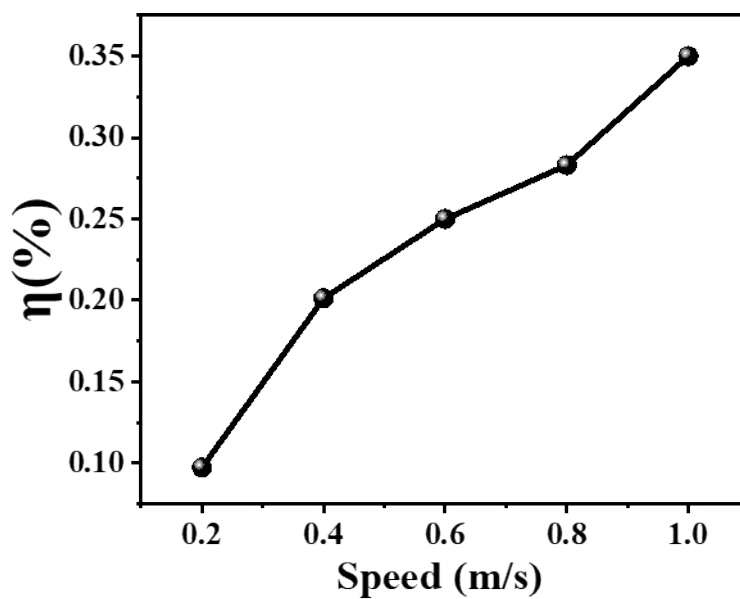
Figure S15. Average energy conversion efficiency of the FDC-TENG at different speeds.
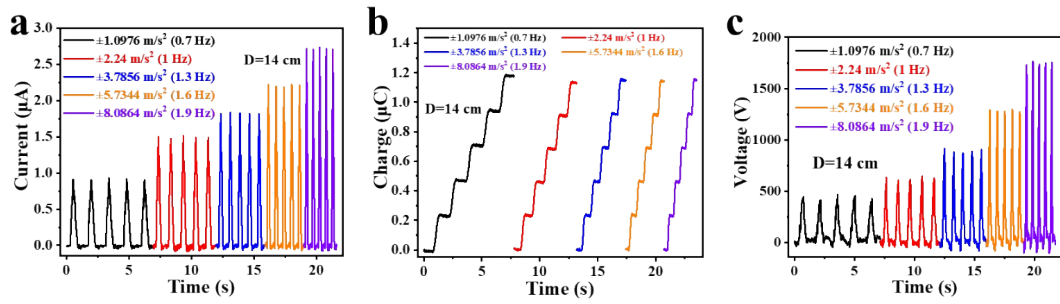
Figure S16. The current (a), charge transfer (b), and voltage (c) of the FDC-TENG with different acceleration and deceleration.
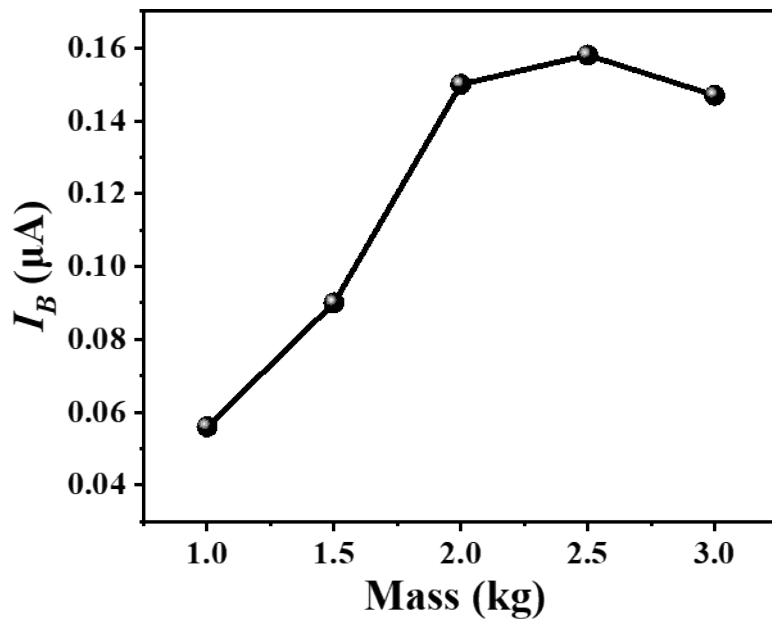
Figure S17. Variation of the reverse current I_B of the FDC-TENG under different weights. The values of I_B in the range of 0.2-0.7 kg are too small to count, and not shown in the curve.
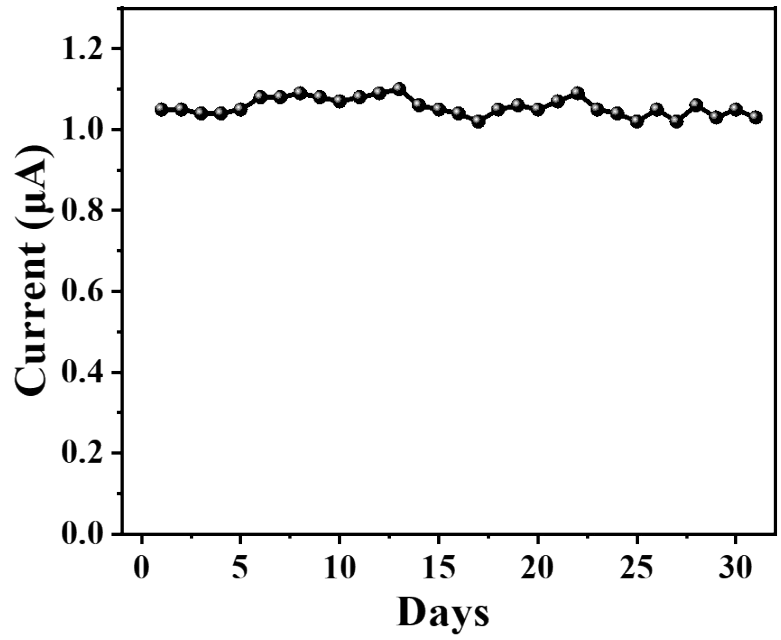
Figure S18. Analyses of the stability and durability of the FDC-TENG during one month of intermittent loading.
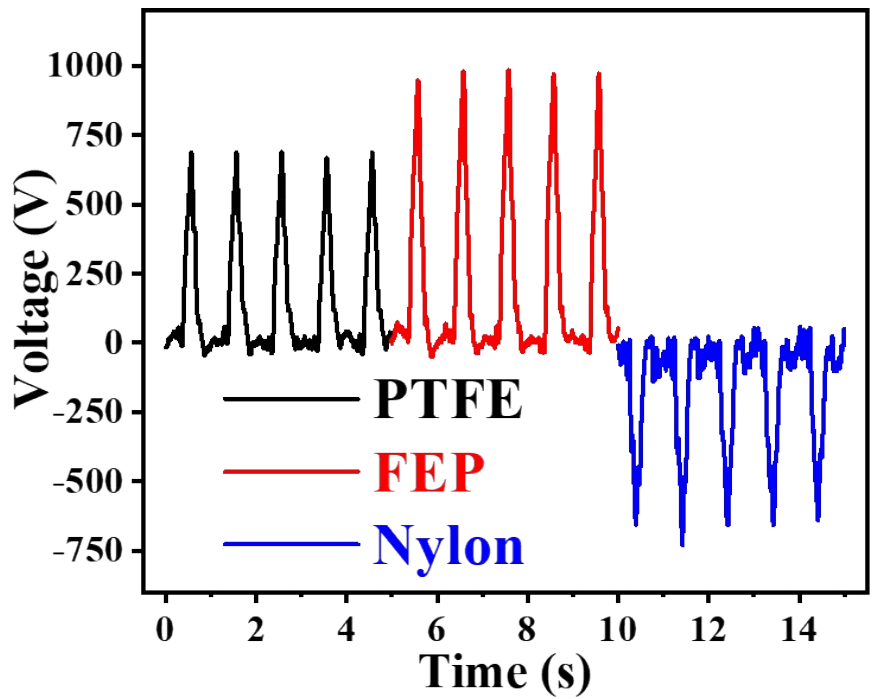
Figure S19. The voltage when the FDC-TENG sliding on PTFE, FEP, and nylon.
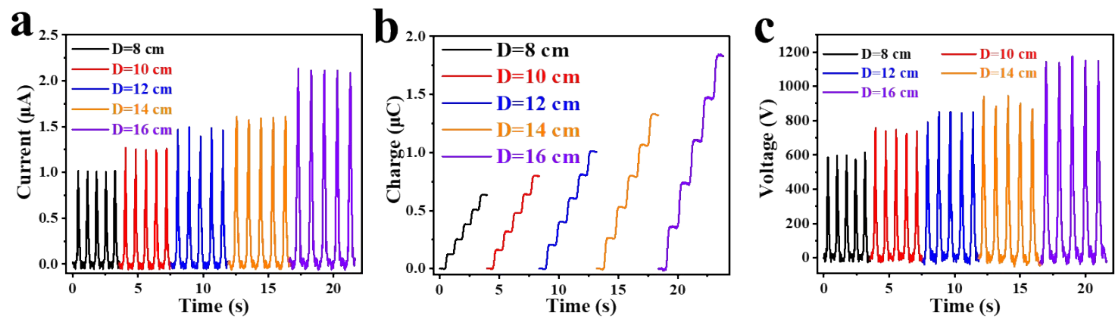
Figure S20. Variation of the current (a), charge transfer (b), and voltage (c) of the FDC-TENG with different *D* values.
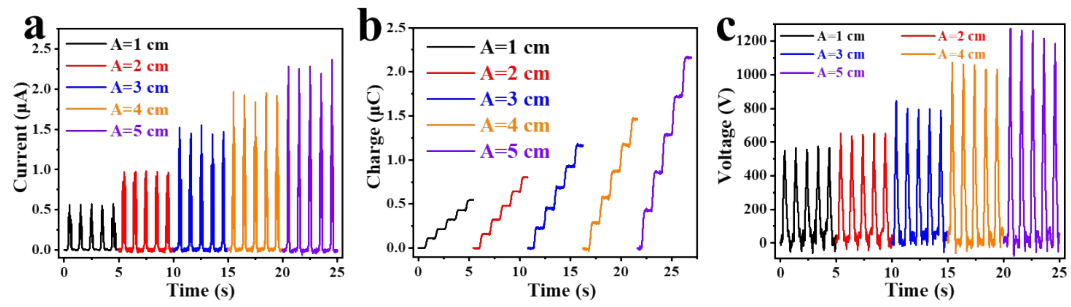
Figure S21. Effect of *A* on the current (a), charge transfer (b), and voltage (c).
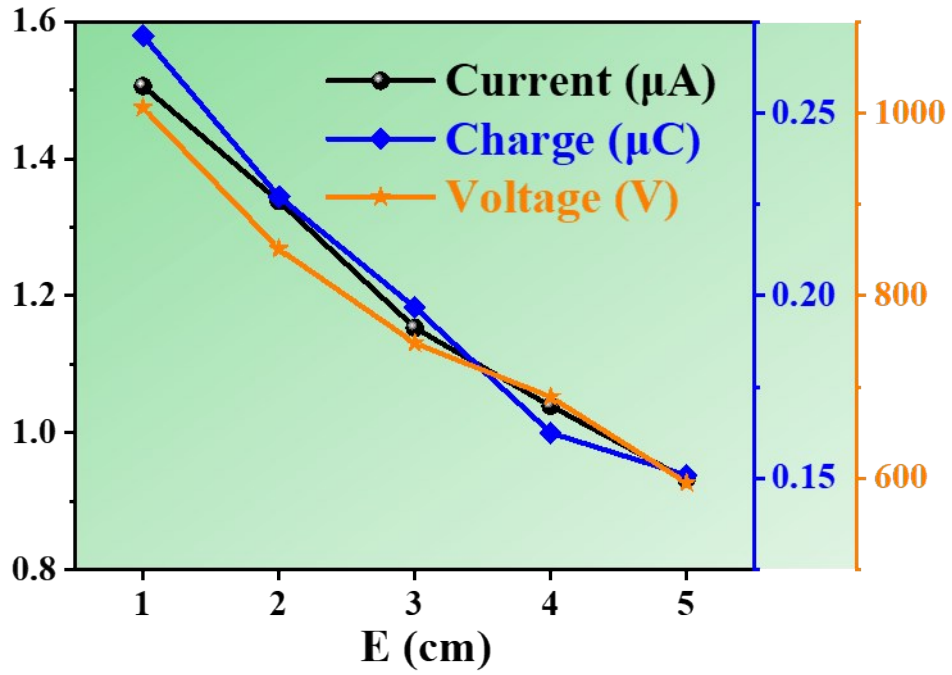
Figure S22. The electrical output of the FDC-TENG with different *E* values.
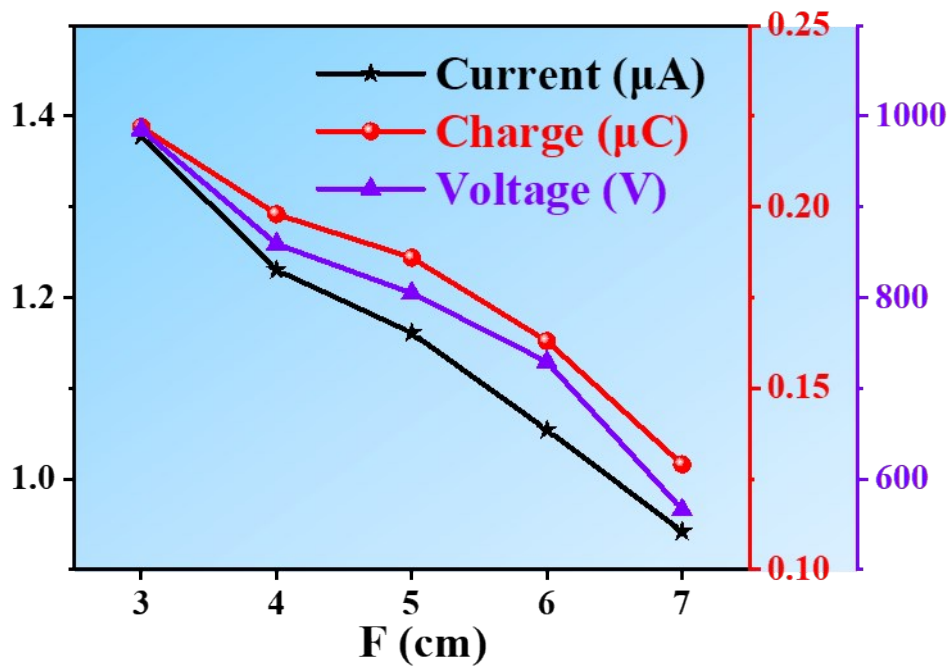
Figure S23. The relationship between the output performance and *F* values.
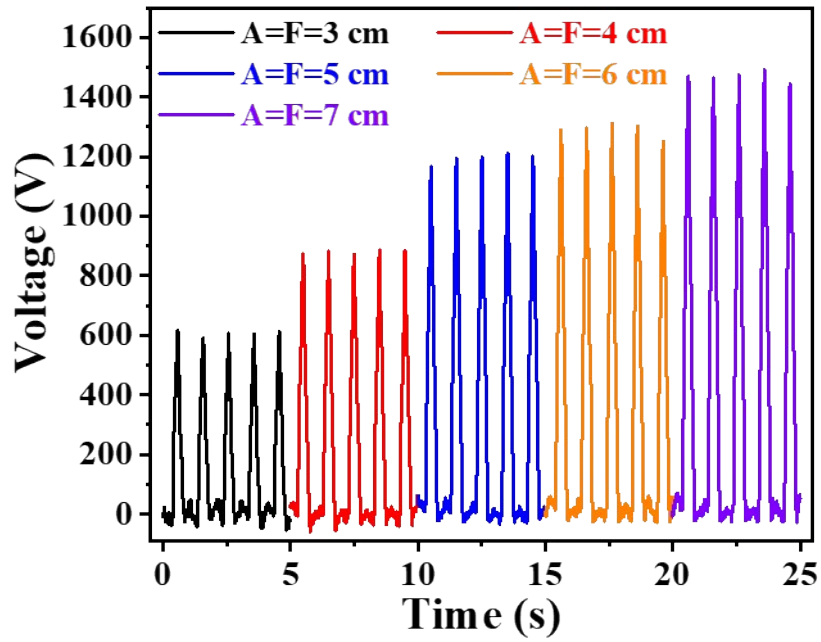
Figure S24. The voltage of the FDC-TENG with different *A* and *F* values (A=F).
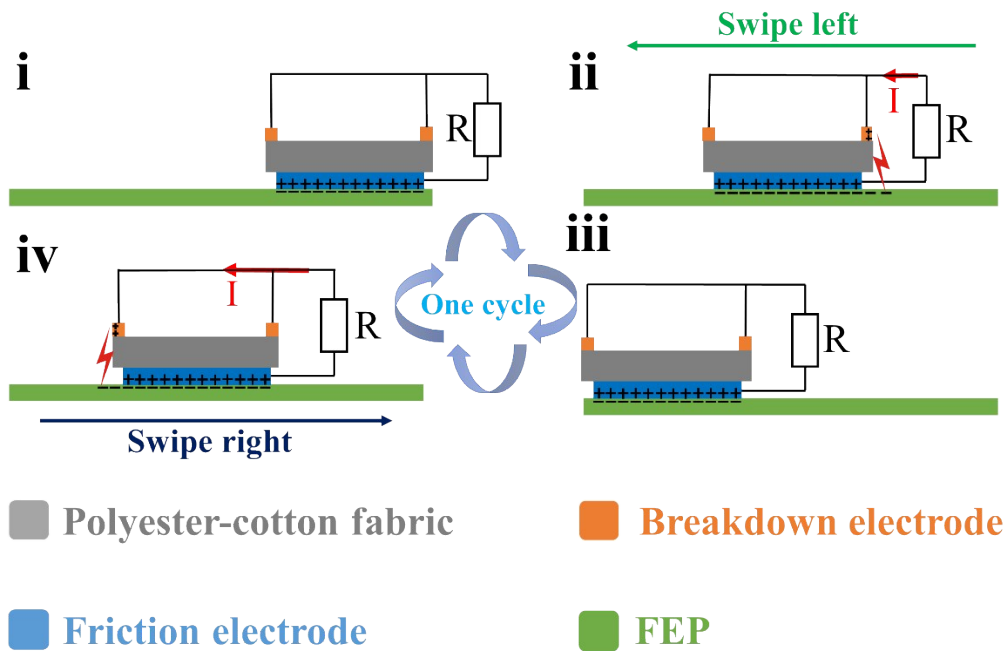
Figure S25. Schematic of the working mechanism of the FDC-TENG with two breakdown electrodes.
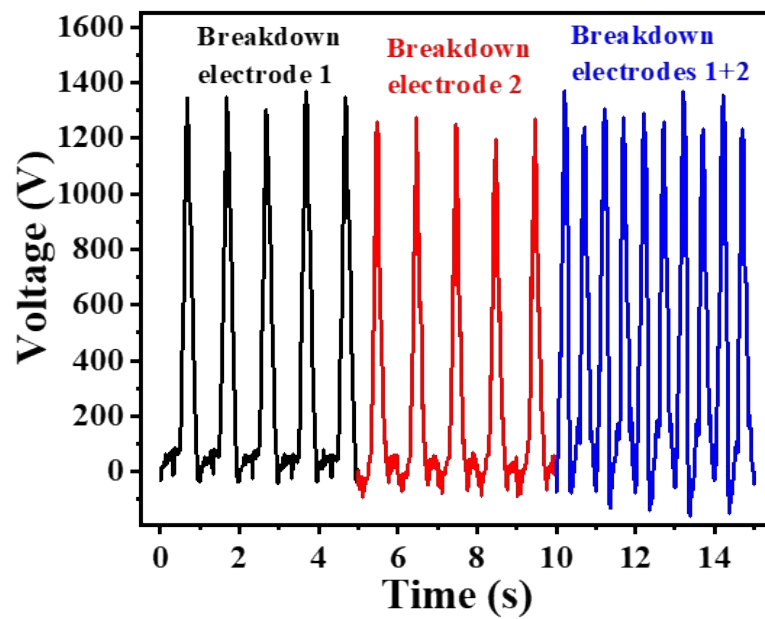
Figure S26. The voltage of the FDC-TENG with two breakdown electrodes in different connection modes.
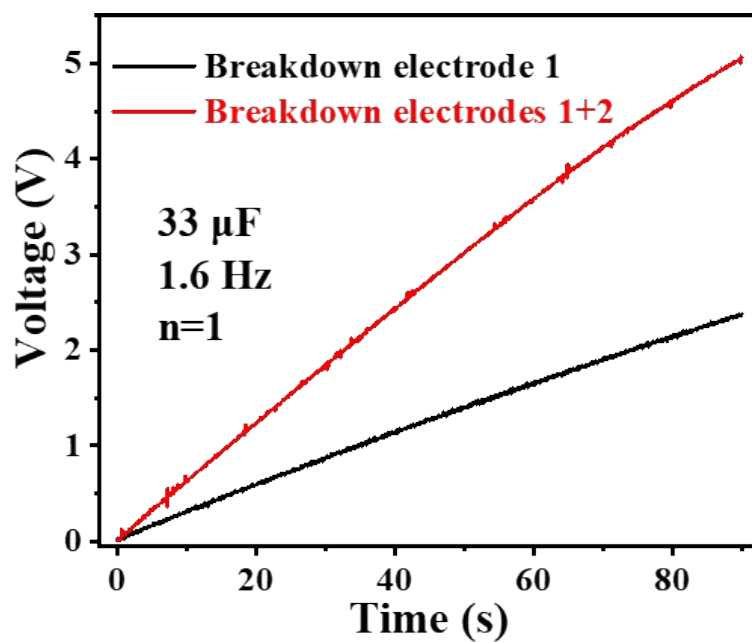
Figure S27. Charging voltage curves of the FDC-TENG for 33 µF electrolytic capacitor with one breakdown electrode and two breakdown electrodes.
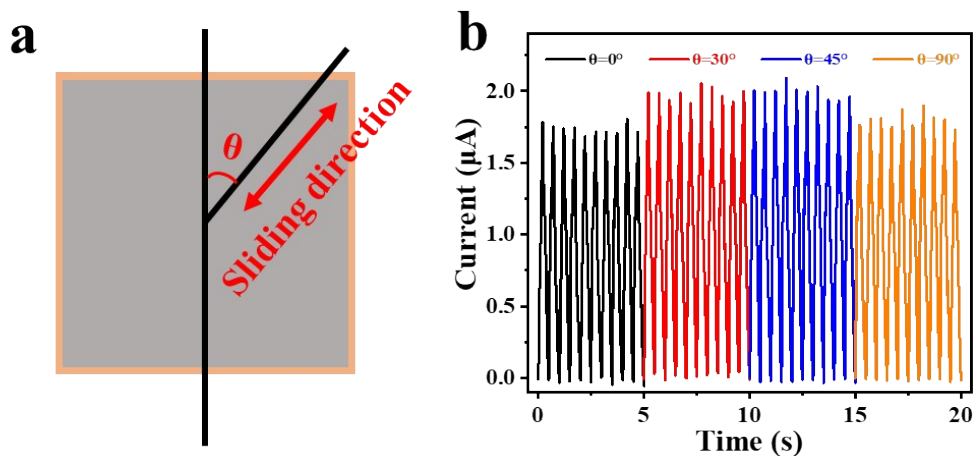
Figure S28. Schematic diagram (a) and electrical output (b) of the FDC-TENG under different sliding directions.
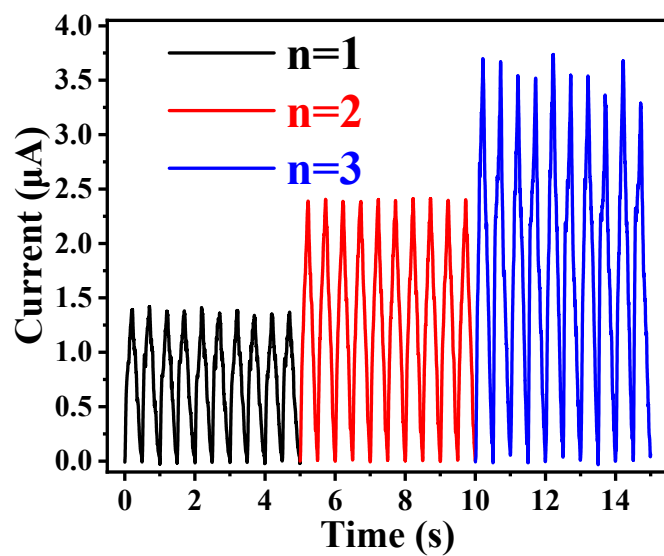
Figure S29. Output current of the FDC-TENG under different number of units.
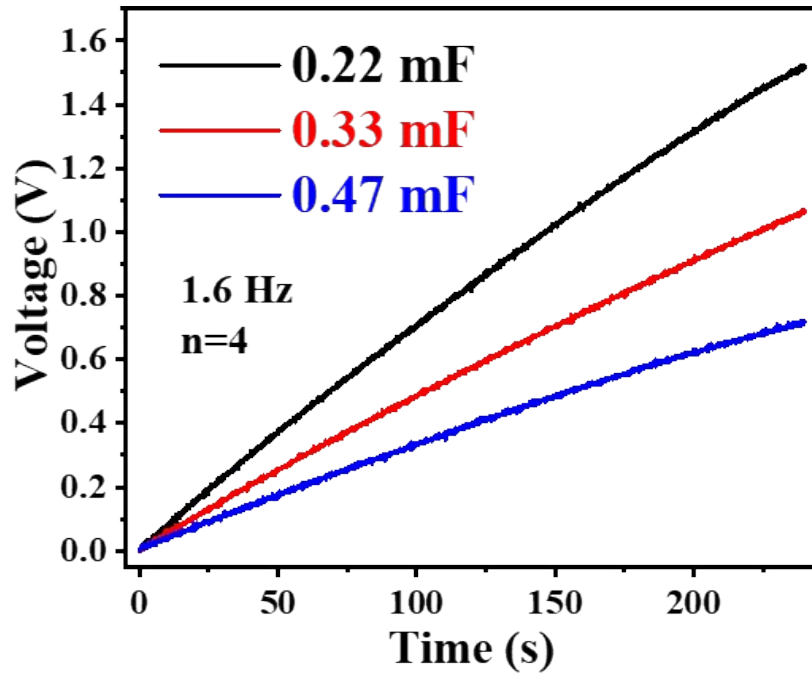
Figure S30. Charging voltage curves of the FDC-TENG for different electrolytic capacitors.
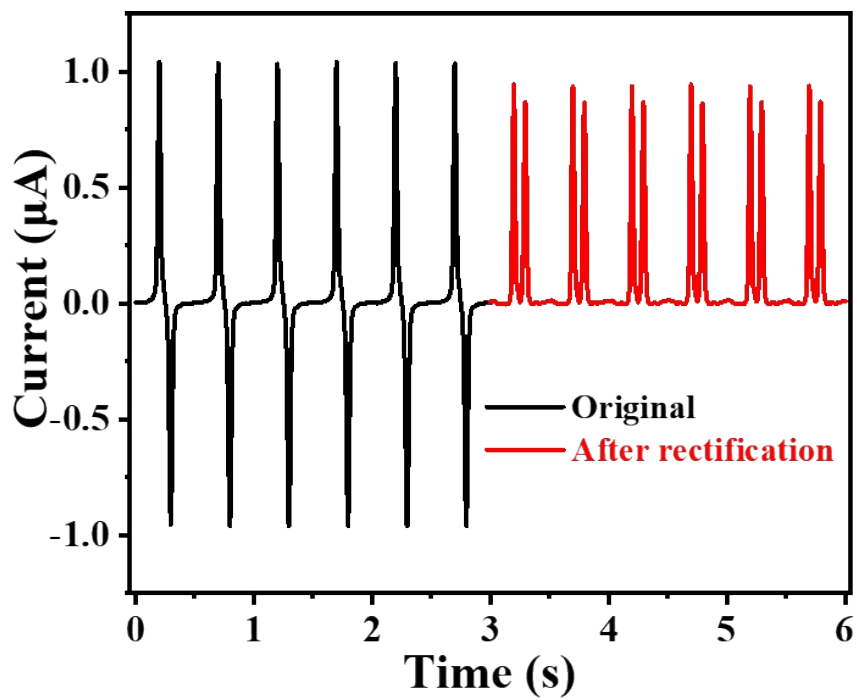
Figure S31. The current before and after rectification.

Note S1. The measurement methods of generated charge density and residual charge density on the FEP film.

As for the generated charge density on the FEP film. Owing to the strong charge dissipation in high surface charge density, it is necessary to measure it as quickly as possible to reduce the impact of charge dissipation. Moreover, when a new electrode material is in contact with the FEP film, the new charge transfer will increase the measurement error. Considering the above factors, the method in Figure S9a is adopted to measure the generated charges. Firstly, the FDC-TENG slides left and right on the FEP film to saturate the surface charge density. After several cycles, separating the FDC-TENG and the FEP film. The surface charges of the contact surface can be measured by the meter. The measurement method for the residual charge density is shown in Figure S9b. The residual charges can be obtained by measuring the transferred induced charges. This method will cause new contact-electrification. However, since the FEP film with residual charges is not in contact with other object, a new charge transfer caused by the contact between FEP film and other object is inevitable.

Note S2. The working mechanism of the FDC-TENG with long width of the breakdown electrode.

Above all, we assume the original surface charge density, the surface charge density after rubbing with the friction electrode, and the surface charge density after harvesting by breakdown electrode of the FEP film are σ_0, σ_2 and σ_1, respectively, where $|\sigma_2|>|\sigma_0|$, $|\sigma_2|>|\sigma_1|$. Initially, the surface of the FEP film and the friction electrode will be charged with the same number of opposite charges. The electrons will exist on the surface of the FEP film due to its stronger capture ability (Figure S10i). When the sliding distance x of the FDC-TENG is less than the width of breakdown electrode (defined as C), the electrostatic field generated by σ_2 is almost

impossible to cause electrostatic breakdown between the breakdown electrode and FEP film, due to the existence of a solid polyester-cotton fabric. Owing to $|\sigma_2|>|\sigma_0|$, an induced current I_0 will appear in the external circuit from friction electrode to breakdown electrode until $x=C$ (Figure S10ii). There will be an air-only area between breakdown electrode and FEP film with a relatively low critical breakdown field strength (~ 3 kV mm^{-1} from Paschen's law). The strong electrostatic field between the breakdown electrode and FEP film that caused by σ_2 will break down the air to generate a conductive plasma channel, and a big current I_A will exist in the external circuit from friction electrode to breakdown electrode (Figure S10iii). Owing to the barrier of polyester-cotton fabric, the tribo-charges on the FEP film that directly under the breakdown electrode are not harvested (Figure S10iv). However, the charges in the left of breakdown electrode can be effectively harvested. An induced current I_B will exist in the external circuit from breakdown electrode to friction electrode, due to the absolute value of σ_2 is greater than that of σ_1 (Figure S10v). After that, there will be no current in the external circuit when the FDC-TENG slides to the left (Figure S10vi).

Note S3. The calculation method of average energy conversion efficiency.

The average energy conversion efficiency η is defined as the ratio of generated electricity by FDC-TENG W_0 and the input mechanical energy E_k,

$$\eta = \frac{W_0}{E_k} \qquad (1)$$

which can be further expressed as

$$\eta = \frac{\int_0^T I^2 R_0 dt}{\int_0^x F dx} \qquad (2)$$

where R_0 is the external resistance, I is the output current, F is the external force. When FDC-TENG is moving at a constant speed, $F=f$. Where f is the sliding friction force, which can be expressed as

$$f=\mu N \qquad (3)$$

μ is dynamic friction factor and N is the pressure on contact surface. According to formula (3), the external force F remains constant as the FDC-TENG slides at a constant speed. And $F=f=3.58$ N when applying 2 kg weight on the FDC-TENG. Therefore, the average energy conversion efficiency η can be obtained through measuring the output current I at different speeds.

Note S4. The electrical output of the FDC-TENG with two breakdown electrodes on the edges.

The working principle of FDC-TENG with single breakdown electrode has been illustrated in Figure 1c in detail. It can be found that there is a large number of tribo-charges on the surface of the FEP film in the right side of the FDC-TENG when sliding it to the left. However, these charges cannot be harvested due to the lack of a breakdown electrode on the right edge of the polyester-cotton fabric. Therefore, the wasted energy can be harvested if another breakdown electrode is also arranged on the right edge. The working mechanism is the same as we analyzed in Figure 1c. The difference is that air breakdown will occur in both sliding processes (Figure S25ii and iv). Therefore, this improvement on structure can double the electrical output.